



**HAL**  
open science

## Investigations on the Diffusion of Oxygen in Nickel at 1000°C by SIMS Analysis

Simon Perusin, Daniel Monceau, Eric Andrieu

► **To cite this version:**

Simon Perusin, Daniel Monceau, Eric Andrieu. Investigations on the Diffusion of Oxygen in Nickel at 1000°C by SIMS Analysis. *Journal of The Electrochemical Society*, 2005, 152 (12), pp.390-397. 10.1149/1.2116787 . hal-03600387

**HAL Id: hal-03600387**

**<https://hal.science/hal-03600387>**

Submitted on 7 Mar 2022

**HAL** is a multi-disciplinary open access archive for the deposit and dissemination of scientific research documents, whether they are published or not. The documents may come from teaching and research institutions in France or abroad, or from public or private research centers.

L'archive ouverte pluridisciplinaire **HAL**, est destinée au dépôt et à la diffusion de documents scientifiques de niveau recherche, publiés ou non, émanant des établissements d'enseignement et de recherche français ou étrangers, des laboratoires publics ou privés.



## Open Archive Toulouse Archive Ouverte (OATAO)

OATAO is an open access repository that collects the work of Toulouse researchers and makes it freely available over the web where possible.

This is an author-deposited version published in: <http://oatao.univ-toulouse.fr/>  
Eprints ID : 2701

**To link to this article :**

URL : <http://dx.doi.org/10.1149/1.2116787>

**To cite this version :** Pérusin, Simon and Monceau, Daniel and Andrieu, Eric (2005) *[Investigations on the Diffusion of Oxygen in Nickel at 1000°C by SIMS Analysis](#)*. Journal of The Electrochemical Society (JES), vol. 152 (n° 12). pp. E390-E397. ISSN 0013-4651

Any correspondence concerning this service should be sent to the repository administrator: [staff-oatao@inp-toulouse.fr](mailto:staff-oatao@inp-toulouse.fr)

# Investigations on the Diffusion of Oxygen in Nickel at 1000°C by SIMS Analysis

Simon Perusin,<sup>z</sup> Daniel Monceau,<sup>a</sup> and Eric Andrieu

CIRIMAT UMR 5085, ENSIACET-INPT, 31077 Toulouse Cedex 4, France

High-purity polycrystalline nickel foils have been oxidized at 1000°C in laboratory air before being analyzed in secondary ion mass spectrometry to locally measure the oxygen content in solid solution. The values obtained in metallic grains are surprisingly the same before and after the oxidation treatments (between 5 and 10 atom ppm) and they are much lower than the ones predicted from the literature solubility and diffusion coefficient data at 1000°C. It is shown that this discrepancy could have its origins in the purity level of the samples but also in the exclusive oxygen diffusion in nickel grain boundaries. This last assumption is supported by the occurrence of nickel oxide particles on the walls of voids located in grain boundaries.

DOI: 10.1149/1.2116787

The influence of chemical environment on mechanical properties and behavior of nickel alloys can be illustrated by many examples. At high temperature, many nickel-based alloys show a dramatic reduction in tensile ductility in the range 700–900°C after short exposures in air at about 1000°C.<sup>1–3</sup> This ductility loss is often associated with intergranular fracture. Bricknell et al. have demonstrated that the ductility minimum observed in pure nickel (polycrystal Ni270) at 800°C was imputable to the oxygen species.<sup>3,4</sup> At this temperature, grain boundary sliding in polycrystalline nickel is an operative mechanism of plastic deformation of the metal if the necessary accommodation mechanisms for grain boundary sliding can operate (elastic distortion, dislocations movement, and diffusion). An embrittlement mechanism which relies on a lack of accommodation for grain boundary sliding has been suggested. In high-purity nickel, oxygen segregation in metallic grain boundaries has been proposed as the effective mechanism for the grain boundaries pinning but no successful quantification of this segregation has been reported.

At low temperature in hot water, cracking of Ni-base alloys at low electrochemical potentials was observed<sup>5–7</sup> (potentials close to the Ni/NiO equilibrium) but the environmental mechanism responsible for the crack propagation is not yet understood. The crack propagation rate exhibits a high activation energy similar to solid-state diffusion: this experimental fact has motivated theories for internal oxidation based on the kinetics of grain boundary oxygen diffusion. However, no direct measurement of the diffusion of oxygen in solid solution has been realized. Recent developments in chemical analysis should be of great interest to investigate the oxygen diffusion and solubility in nickel: due to its high sensitivity, secondary ion mass spectrometry (SIMS) is a powerful technique to tackle this subject.

The solubility of oxygen in nickel between 600 and 1200°C was first reported by Seybolt and Fullman.<sup>8</sup> Their method involved first oxidizing the surface of a pure nickel sheet and then equilibrating the metal and metal oxide in a slightly oxidizing atmosphere. After the superficial oxide layer had been removed, the metal was chemically analyzed for oxygen. Alcock and Brown<sup>9</sup> used a thermogravimetric method in which the oxygen fugacity was maintained by a CO<sub>2</sub>/CO gas mixture: the weight change of a nickel sample was then measured as a function of the fugacity. However, in both cases, the authors measured a decrease in the solubility (Fig. 1) with increasing temperature, in contrast to most metal–oxygen systems. Then, doubts can be expressed about these results.

The most complete work on this subject was realized by Park and Alstetter<sup>10</sup> using electrochemical techniques in which oxygen concentration is controlled by coulometric titration. The experiments

were carried out between 800 and 1000°C leading to the following equation for the solubility of oxygen in solid nickel

$$C_o^s = 8.3 \begin{pmatrix} +5.1 \\ -3.5 \end{pmatrix} \exp\left(-\frac{55 \pm 1.3}{RT} \text{kJ/mol}\right) \text{ atom \%}$$

Note that in this case, the solubility increases with increasing temperature (Fig. 1).

To determine the diffusivity of oxygen in nickel, measurements of the permeability of oxygen in nickel, i.e., the product of the solubility and the diffusivity, were first made<sup>11–17</sup> using the internal oxidation method in Ni–Si,<sup>11</sup> Ni–Cr,<sup>12</sup> or Ni–Be alloys.<sup>13,14</sup> To calculate the diffusivity from the permeability, the solubility data of Seybolt<sup>8</sup> were used in the above works except for Smithells and Ransley,<sup>16</sup> who used a constant value of 600 at ppm for the solubility.

Alcock and Brown<sup>9</sup> measured the time required to reach equilibrium at each temperature to calculate approximate diffusion coefficients from thermogravimetric measurements.

Park and Alstetter<sup>10</sup> used an electrochemical technique. This work is the only one in which an independent determination of the diffusivity of oxygen in nickel between 800 and 1000°C has been made.

All these results are compiled in Fig. 2: one can first notice that the diffusivity values obtained by the internal oxidation method are close to each other in the temperature range 800–1200°C except for the Lloyd and Martin results.<sup>13,14</sup> The second remark concerns the activation energy of diffusion: the value obtained by Park and Alstetter<sup>10</sup> is much lower than the ones achieved with the internal oxidation method. This discrepancy finds its origin in the values of

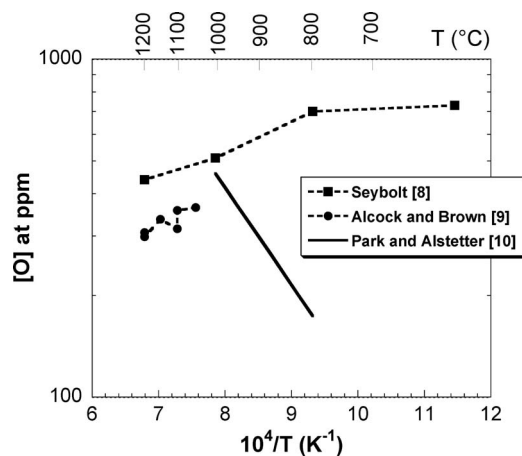
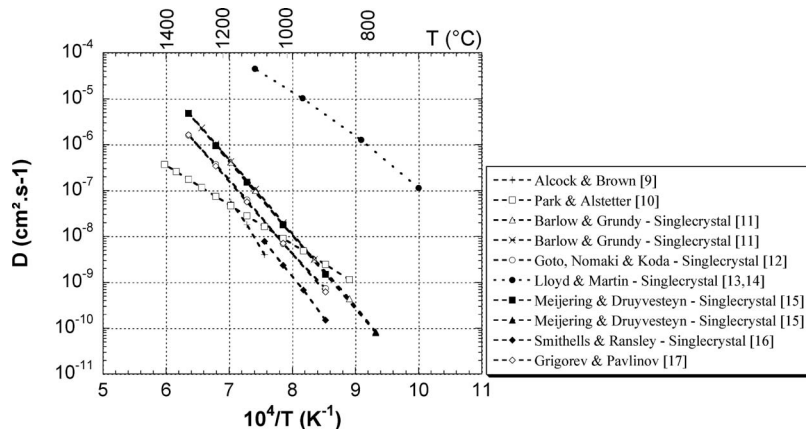


Figure 1. Solubility of oxygen in solid nickel at high temperature (literature data).

<sup>a</sup> Present address: School of Material Science and Engineering, University of New South Wales, Sydney, Australia.

<sup>z</sup> E-mail: Simon.Perusin@ensiacet.fr



**Figure 2.** Diffusivity of oxygen in solid nickel at high temperature (literature data).

the oxygen solubility used by the authors to calculate the diffusion coefficient from the permeability measurements: in the internal oxidation method studies, the oxygen solubility determined by Seybolt et al.<sup>8</sup> decreases with increasing temperature, whereas it increases with temperature for the Park and Alstetter work.<sup>10</sup> Nevertheless, at the temperature of 1000°C chosen for the present study, the terminal solubility of oxygen in nickel is found to be about the same by Seybolt et al. and by Park et al. As a consequence, the value of the oxygen diffusion coefficient as determined by Park and Alstetter is also close to the values found in the internal oxidation studies, at 1000°C.

#### Calculation of the Oxygen Diffusion at 1000°C from Literature Data

In a nonpermanent regime and without any external force, when  $D$  is independent of the concentration, which is the case for oxygen in nickel (the solubility of oxygen being low), Fick's second law is written

$$\frac{\partial C}{\partial t} = D \frac{\partial^2 C}{\partial x^2} \quad [1]$$

where  $C$  and  $D$  are, respectively, the concentration and the diffusion coefficient of the diffusing species (oxygen in our case), considering the diffusion in one direction. Equation 1 was numerically solved using Mathematica® software, which represents numerical approximations to functions as interpolating function objects. To calculate these functions, the diffusion coefficient  $D$  and the solubility  $C_s$  obtained by Park and Alstetter<sup>10</sup> at 1000°C were used (i.e.,  $D = 9.13 \times 10^{-9} \text{ cm}^2 \text{ s}^{-1}$  and  $C_s = 460$  at ppm). Results obtained for two thicknesses of samples (1 mm and 125  $\mu\text{m}$ ) are shown in Fig. 3. This figure points out that oxygen diffusion at this temperature is very fast so that relatively short oxidation treatments should be necessary to reach the solubility limit for oxygen in the middle of

the nickel foil (about 2 h for the 125- $\mu\text{m}$ -thick foil and about 100 h for the 1-mm-thick one).

These calculations from the literature data show that it should be feasible to use the direct analysis provided by the SIMS and GDMS techniques to determine the oxygen diffusion coefficient and its solubility in nickel after heat-treatments of the samples.

#### Materials and High-Temperature Treatments

The investigations were realized on high-purity polycrystalline nickel foils, 125  $\mu\text{m}$  and 1 mm thick. The mean grain size of the as-received materials (determined by image analysis) was around 50  $\mu\text{m}$  for the 1-mm-thick foil and 35  $\mu\text{m}$  for the 125  $\mu\text{m}$  one. Surface preparation is well known to play a great role in the oxidation kinetics and oxide morphologies.<sup>18,19</sup> Moreover, as will be shown later, the surface roughness has a strong effect on the depth profiles obtained using the SIMS technique. As a consequence, foils were carefully polished down to 1  $\mu\text{m}$  by using diamond paste. After cleaning in acetone and then in ethanol using ultrasonic waves (30 s for each solvent), the samples were annealed in a dry mixture of argon and hydrogen (5 vol %  $\text{H}_2$ ) at 1000°C for 1 h to stabilize the microstructure (or at least to slow down subsequent grain growth). The gas pressure in the furnace is equal to 1.5 bar.

Hydrogen content after annealing was not checked. But the partial pressure of hydrogen in the furnace (about 7500 Pa) is many times lower than the pressures commonly used to hydrogenate nickel (a few GPa). Moreover, the samples are cooled down in the argon-hydrogen mixture: as the solubility of hydrogen in nickel at room temperature is about 1 atom ppm under a hydrogen pressure of  $10^5 \text{ Pa}$ ,<sup>20</sup> one can assess that the hydrogen content in the heat-treated samples is lower than 1 atom ppm.

The chemical compositions of the two types of samples were then determined by glow discharge mass spectrometry (GDMS) (Table I). From an internal oxidation point of view,<sup>21,22</sup> the nickel

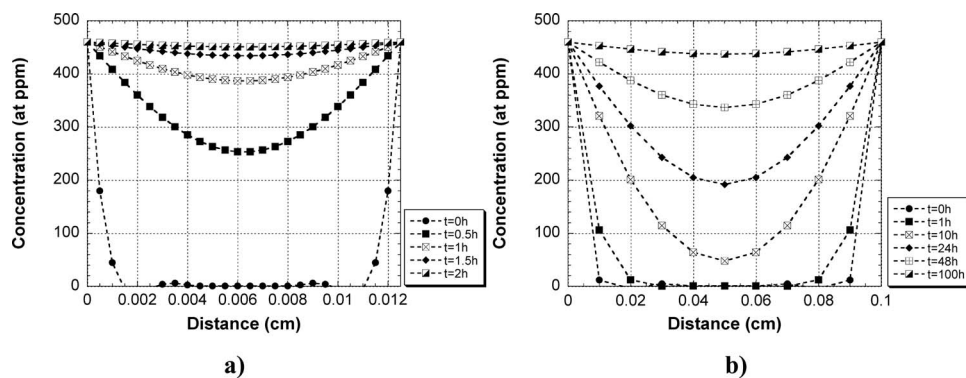


**Figure 3.** Calculations of the oxygen diffusivity in solid nickel at 1000°C as a function of time. (a) 125- $\mu\text{m}$ -thick foil, (b) 1-mm-thick foil. The diffusion coefficient  $D$  ( $D = 9.13 \times 10^{-9} \text{ cm}^2 \text{ s}^{-1}$ ) and the solubility  $C_s$  ( $C_s = 460$  at ppm) obtained by Park and Alstetter<sup>10</sup> at 1000°C were used for the calculations.

**Table I. Chemical composition of the nickel foils after heat-treatment in a mixture of argon and hydrogen (5 vol % H<sub>2</sub>)-1 h/1000°C-atom ppm.**

Element	Co	Cr	Cu	Fe	Mg	Mn	Si	Ti	C	S	O	N	Ni
Foil A (e = 125 μm)	8	9	9	12	24	10	15	12	0.49	0.4	5	0.17	bal
Foil B (e = 1 mm)	0.06	0.09	0.08	0.55	0.001	0.007	0.42	0.01	4.8	0.73	10	10	bal

should behave as a pure metal alloyed with only 78 atom ppm of total metallic impurities (Co, Cr, Fe, Mg, Mn, Si, Ti) able to form an oxide more stable than nickel oxide, for the thin foil (125 μm), and less than 1 atom ppm for the thick foil (1 mm). Note, finally, that the mean grain size obtained after heat-treatment was in the range 350–450 μm.

Oxidation treatments were then realized at 1000°C in laboratory air using a classical resistance furnace. For the Ni/NiO system, the oxide scale–metal adhesion is recognized to be excellent for flat surfaces.<sup>23–25</sup> Indeed, we did not observe any spallation either on thick specimens or on thin ones. Three oxidation treatments were given: the thinnest foil (125 μm) was oxidized 1 and 100 h in laboratory air and the thickest one 48 h also in laboratory air. According to direct observations of cross sections of oxidized samples and estimations made from weight-gain curves, the average thickness of the NiO scale is about 5 μm after 1 h at 1000°C, 35 μm after 48 h, and 43 μm after 100 h, which is in quite good agreement with previous results.<sup>26,27</sup> In each case, the scale consists of an inner layer of equiaxed grains showing few voids and a compact outer layer of columnar grains,<sup>28</sup> i.e., a duplex scale microstructure which was not observed for temperatures higher than 800°C.<sup>25,26</sup> This difference could be due to the fact that the present samples were oxidized in laboratory air instead of oxygen, the purity level of the present thick foil and its surface preparation being similar to that of the nickel samples used in previous works.<sup>25,26</sup>

### Analytical Study

*SIMS calibrations.*—SIMS depth profiling is a surface analysis technique capable of determining the elemental concentrations of dopant and impurity atoms within a material as a function of depth. The technique is used to determine concentrations in the range of 10<sup>13</sup>–10<sup>20</sup> atoms cm<sup>-3</sup> lying at depths of up to 10 μm. The secondary ionic intensity received from the sample is usually plotted as a function of sputter time. To generate a SIMS concentration depth profile, calibrations are required and are listed below.

To convert the time axis into depth in the case of pure nickel, an optical profilometer ZYGO New View 100 was used to measure the sputter crater depth after each SIMS analysis. Total crater depth divided by total sputter time then provides the average sputter rate. Depth resolution depends on flat bottom craters. Note that the SIMS instrument used provides uniform sputter currents by sweeping a finely focused primary beam in a raster pattern over a square area. Apertures select secondary ions from the crater's bottom but not from the edges, which are not flat. Craters of 80 × 80 μm<sup>2</sup> were realized by using a Cs<sup>+</sup> primary beam of 100 nA and 1.7 kV. A mean sputter rate of 154 Å/s can be deduced from interferometry analysis with a maximum uncertainty of 10 Å/s, which is due to the dispersion of the results and the roughness of the bottom of the craters.

The conversion of intensity into concentration was only realized for oxygen in solid solution in nickel. Indeed, when the concentration of an element is low (<1%), which is obviously the case for oxygen in nickel, the relationship between intensity and concentration is linear.<sup>29</sup> As the material used in the present work is of high purity, a calibration can be made on a test block in which the concentration in oxygen is known. This was done on the Ar–H<sub>2</sub> annealed nickel foils in which the oxygen concentration in the bulk

was obtained by GDMS (Table I): values of 5 and 10 atom ppm were measured for the two types of samples A and B. Then the calibration factor  $k_O$  is defined as

$$k_O = C_O^{\text{ref}} \frac{I_{\text{Ni}}^{\text{ref}}}{I_{\text{O}}^{\text{ref}}} \quad [2]$$

where  $C_O^{\text{ref}}$  is the concentration of oxygen in nickel in the annealed sample and  $I_{\text{Ni}}^{\text{ref}}$ ,  $I_{\text{O}}^{\text{ref}}$  the intensities of nickel and oxygen signals, respectively. In the case of a Cs<sup>+</sup> primary current of (100 nA–1.7 kV), and for a raster size of 80 × 80 μm with a field aperture of 8 μm, a value of 1800 (±200) was found for  $k_O$  using atom ppm units for  $C_O^{\text{ref}}$ . This value was confirmed by GDMS and SIMS analysis made on a (111) single crystal of nickel in which the oxygen content (10 atom ppm) had been given by the producer.

Because of this calibration, the concentration of oxygen in a sample treated at high temperature can be calculated at any point in the bulk using the equation

$$C_O = k_O \frac{I_O}{I_{\text{Ni}}} \quad [3]$$

where  $C_O$  is the concentration of oxygen in nickel in the oxidized sample and  $I_{\text{Ni}}$ ,  $I_O$  are the intensities of nickel and oxygen signals, respectively. Note that the measurements must be realized, as much as possible, in the same conditions (same source of primary ions, same primary current, same angle of incidence of the primary beam) as for the test block.

The analyses were realized in a CAMECA IMS 4F6 apparatus, which uses Cs<sup>+</sup> ions as primary source. The primary current was fixed to 100 nA and all the profiles presented in this paper have been obtained by using an 80 × 80 μm<sup>2</sup> raster size with an 8 μm field aperture. The detection of <sup>12</sup>C<sup>-</sup>, <sup>14</sup>N<sup>-</sup>, <sup>16</sup>O<sup>-</sup>, <sup>32</sup>S<sup>-</sup>, <sup>28</sup>Si<sup>-</sup>, and <sup>58</sup>Ni<sup>-</sup> secondary ions was realized. As the profiles obtained for <sup>12</sup>C<sup>-</sup>, <sup>14</sup>N<sup>-</sup>, <sup>32</sup>S<sup>-</sup>, and <sup>28</sup>Si<sup>-</sup> do not show any peculiar aspect, they are not presented in this study.

*Back-side polishing preparation for SIMS.*—To determine the concentration of one species in an oxidized sample using the SIMS technique, the classical procedure first implies the sputtering of the

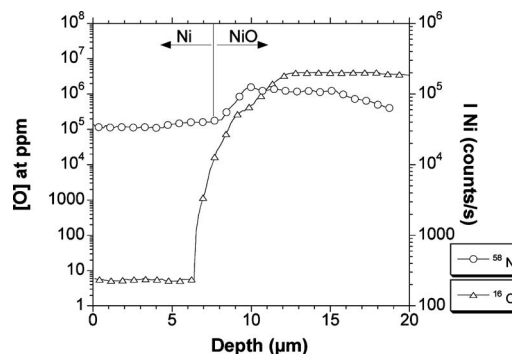


**Figure 4.** Reverse side SIMS profiles of <sup>16</sup>O and <sup>54</sup>Ni obtained in a 125-μm-thick nickel foil–1 h/1000°C/laboratory air. Profiles obtained in a metallic grain.

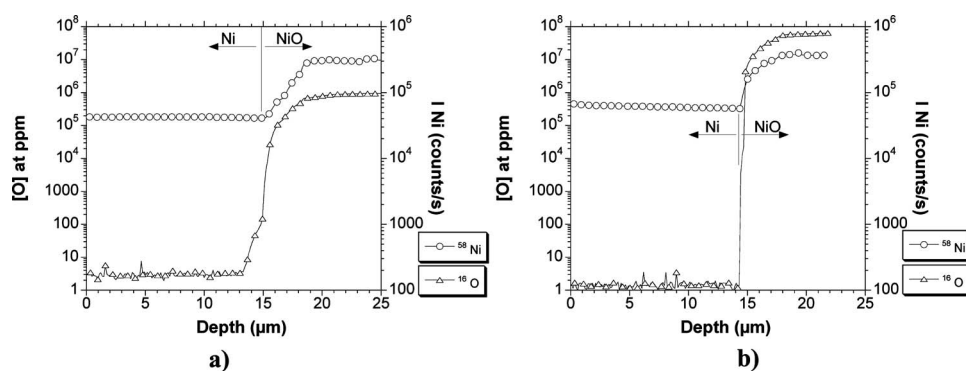


**Figure 5.** Reverse side SIMS profiles of  $^{16}\text{O}$  and  $^{58}\text{Ni}$  obtained in a 125- $\mu\text{m}$ -thick nickel foil—100 h/1000°C/laboratory air. (a) Profiles obtained in a metallic grain, (b) profiles obtained in a metallic grain boundary.

oxide scale and then the sputtering of the substrate.<sup>30</sup> In our case, however, this technique presents numerous drawbacks.

The mean grain size of the oxide scale NiO obtained after all the oxidation treatments presented in this paper is really lower than 80  $\mu\text{m}$  (about 5  $\mu\text{m}$  after 48 h at 1000°C). Therefore, using a raster size of 80  $\times$  80  $\mu\text{m}$ , the sputtering of numerous oxide grains is made during the depth profiling. Because the sputtering rate depends on the crystallographic orientation, the bottom of the SIMS craters is not flat.

The oxide scale formed at 1000°C is duplex<sup>28,31</sup> with an external layer of columnar grains and an internal layer of equiaxed grains. This internal layer contains a few pores which of course influence the sputtering rate.

Finally, using this technique, it is impossible to focus the primary beam on a metal grain boundary because, in a way, the metal substrate is hidden by the oxide scale.

The first two drawbacks may prevent a correct estimation of the oxygen diffusion in the metal substrate. Indeed, as the bottom of the craters is not flat, the depth resolution is strongly decreased and thus the errors made on the values of the diffusion coefficients are significant. To overcome these problems, a back-side polishing preparation has been developed.<sup>32,33</sup> The sample oxidized on both sides is pasted on a brass cylinder which gives a more manageable system. This system is then ground with 1200 grit SiC paper, using a tube in which the cylinder slides. This procedure allows a regular polishing of the sample. The thickness of the remaining metal is measured using a precision dimpling instrument habitually employed for the preparation of TEM (transmission electron microscopy) specimens. When the sample has reached the desired thickness, final polishing is made using 2400 and 4000 grit papers and then 3 and 1  $\mu\text{m}$  diamond pastes. Then, the paste which has been used to stick the specimen is dissolved in acetone using ultrasonic waves and the sample is rinsed out in ethanol before being carefully placed in the SIMS specimen carrier.

Because of this technique, the SIMS sputtering starts in the metal and is carried on until the metal/oxide scale interface is reached. For

the rest of the paper, the SIMS profiles obtained on samples prepared following the back-side polishing will be called reverse side profiles.

The signal of  $^{58}\text{Ni}$  is used to localize the metal/oxide scale interface. Indeed, it is well known that the sputtering rate of a metallic element is strongly dependent on its chemical bonding<sup>34</sup> and is strongly increased when this element is linked to oxygen in an ionic bonding. As a consequence, in the reverse side profile, the start of the increase of the  $^{58}\text{Ni}$  signal will mark the metal/oxide scale interface.

## Experimental

*125- $\mu\text{m}$ -thick nickel foils.*—The first experiments were realized on 125- $\mu\text{m}$ -thick foils (sample A) oxidized 1 h at 1000°C. According to the Park and Alstetter results<sup>10</sup> and calculations presented before, the oxygen concentration in the oxidized sample should be higher than 400 atom ppm at least 35  $\mu\text{m}$  under the oxide scale-metal interface (see Fig. 3a). However, the SIMS profile obtained in a metallic grain (Fig. 4) shows that the oxygen concentration in the metal has almost not increased after the oxidation treatment in comparison with the initial content in the Ar- $\text{H}_2$  annealed sample: indeed, the concentration is equal to 5 atom ppm after 1 h at 1000°C. Note that the vertical increase of the oxygen signal (after the sputtering of the first 8  $\mu\text{m}$  of metal) is associated with the onset of the metal-oxide scale interface marked out by the increase of the nickel signal (going from  $3 \times 10^4$  to  $1.2 \times 10^5$  counts per second). Then, the diffusion of the oxygen species in the metal cannot be suspected at least on distances higher than 1  $\mu\text{m}$ .

The goal of the second oxidation treatment of the thinnest foil (100 h at 1000°C) was to saturate the substrate with oxygen and then to get the terminal solubility of oxygen (i.e., 460 atom ppm from literature results<sup>10</sup>) in the whole sample. The result (Fig. 5a) is again very surprising: the oxygen species has not diffused in the

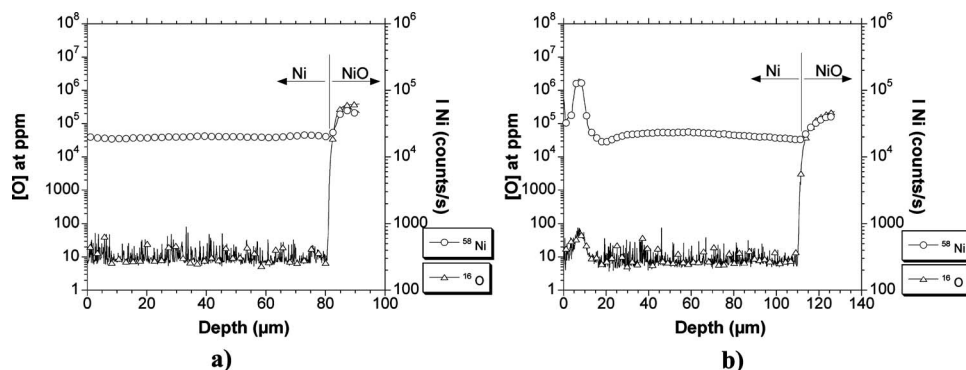


**Figure 6.** Reverse side SIMS profiles of  $^{16}\text{O}$  and  $^{58}\text{Ni}$  obtained in a 1-mm-thick nickel foil-48 h/1000°C/laboratory air. (a) Profiles obtained in a metallic grain, (b) profiles obtained in a metallic grain boundary.

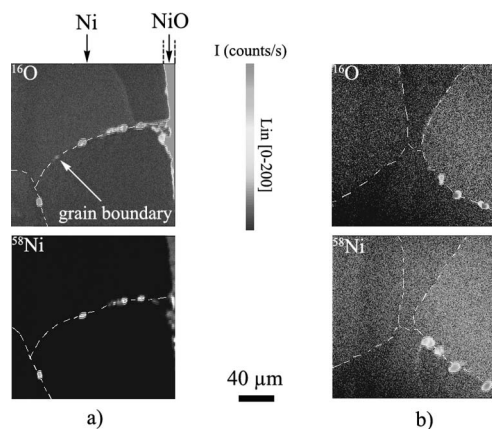


**Figure 7.** SIMS images of  $^{16}\text{O}$  and  $^{58}\text{Ni}$  obtained in 1-mm thick nickel foils oxidized 48 h at  $1000^\circ\text{C}$  in laboratory air cross sections. (a) Metal/oxide scale interface, (b)  $500\ \mu\text{m}$  under the metal/oxide scale interface. Note that, in each case, nickel grain boundaries have been marked by dashed lines.

metal so that its content in the first  $14\ \mu\text{m}$  under the metal-oxide scale interface is again close to 5 atom ppm, i.e., the concentration of oxygen in the Ar- $\text{H}_2$  annealed sample.

As the analysis was only realized in one single grain, the diffusion across the grain boundaries was suspected to explain the literature results. Therefore, sputtering of grain boundaries was realized. The first step to do that is of course the localization of the grain boundaries before the sputtering. The polished samples were then chemically etched in a mixture of nitric acid and acetic acid (50/50 in volume) during 5 s to reveal the microstructure and rinsed out in ethanol before being placed in the SIMS apparatus. Thanks to a video camera, the grain boundaries can be marked out. It is then easy to focus the primary ion beam on the grain boundaries. As the raster size is  $80 \times 80\ \mu\text{m}$  and the field aperture has a  $8\ \mu\text{m}$  diameter, the sputtering of the grain boundary but also of its environment is realized. The SIMS profiles obtained for the sample oxidized 100 h at  $1000^\circ\text{C}$  are presented in Fig. 5b. The results are quite comparable to those achieved for the sputtering of a grain (Fig. 5a): the oxygen species has not diffused in the substrate. Note that the two craters were realized in the same area of the sample: they are indeed  $200\ \mu\text{m}$  apart.

*1-mm-thick nickel foils.*—The same work has been done for thicker samples (1 mm thick, sample B) oxidized 48 h at  $1000^\circ\text{C}$  (Fig. 6). Again, calculations presented in Fig. 3b are not in agreement with the present experimental results: oxygen species has not diffused in the grains of nickel. However, after the oxidation treatment, the different profiles obtained in regions close to grain boundaries have always revealed the presence of surprising isolated oxygen peaks in the metal, as mentioned in Fig. 6b. These peaks are always associated with nickel peaks, which tends to prove the presence of nickel oxide in grain boundaries because the nickel sensibility factor is much higher in NiO than in Ni.

To confirm the presence of nickel oxide, the SIMS apparatus has been used in imaging mode (coupled with sputtering) in which the samples have been prepared by using the classical method for cross sections for the transmission electron microscopy. Indeed, two oxidized samples have been pasted together and polished on their section down to  $1\ \mu\text{m}$  using diamond paste. The samples have then been chemically etched to reveal the grain boundaries (just as presented before for the reverse side method) and placed in the SIMS specimen carrier. Again, thanks to the video camera, the user can easily focus the primary ion beam on a grain boundary. The chosen area is then sputtered and images of the chosen elements ( $^{16}\text{O}$  and  $^{58}\text{Ni}$  in our experiments) can be obtained. The lateral resolution of the images is about  $0.1\ \mu\text{m}$ .

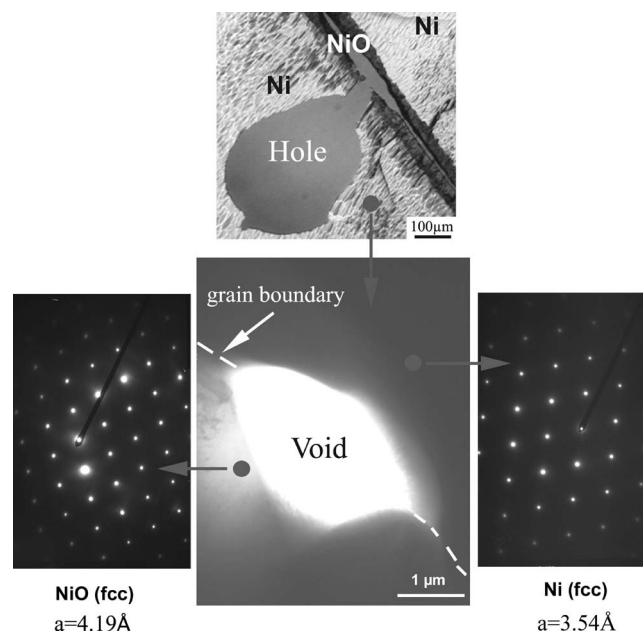


**Figure 8.** Presence of nickel oxide particles in a metallic grain boundary  $200\ \mu\text{m}$  under the metal/oxide scale interface. Nickel foil B oxidized 48 h at  $1000^\circ\text{C}$  in air (TEM investigation).

The chosen raster size was  $256 \times 256\ \mu\text{m}$  to get a quite large area of the section. Figure 7 shows images of  $^{16}\text{O}$  and  $^{58}\text{Ni}$  taken in the nickel substrate. This figure points out areas enriched in oxygen and confined to grain boundaries, which did not exist in the as-received samples. Their mean size is less than  $10\ \mu\text{m}$ . They have been mainly observed at the metal/oxide scale interface (Fig. 7a), but some of them have been localized  $500\ \mu\text{m}$  under this interface (Fig. 7b). After the sputtering of a  $256 \times 256\ \mu\text{m}$  area during 1 h, which approximately corresponds to the removal of  $5\ \mu\text{m}$  of nickel, some of the enriched zones have disappeared but new ones are visible. This latest remark proves that the observations made are not artifacts due to the sample's preparation. Moreover, the signals of other elements such as silicon, carbon, or nitrogen (coming from the pollution of the extreme surface after polishing) have quickly decreased and disappeared after a few minutes of sputtering, whereas the presence of oxygen-enriched areas was still observed. One may well wonder whether this enrichment is due to the presence of nickel oxide or to the presence of oxygen in solid solution. An answer to this question can be given by following the signal of nickel, which is really higher in a region enriched in oxygen than anywhere else (see Fig. 7). As mentioned before, this enhancement of the nickel signal is proof of a change in the nature of the nickel chemical bond; then, these zones are attributed to nickel oxide particles formed during the oxidation treatment.

Moreover, as is shown in Fig. 8, TEM diffraction investigations have confirmed the presence of nickel oxide particles in grain boundaries (as well as energy-dispersive X-ray analysis). Indeed, cross sections of 1-mm-thick nickel foils oxidized 48 h at  $1000^\circ\text{C}$  have been prepared using a precision ion polishing system (PIPS) and nickel oxide particles have been observed as far as  $200\ \mu\text{m}$  under the metal/oxide scale interface. These particles are always located on the walls of voids (Fig. 8); this will be commented on in the Discussion section.

One can then explain the presence of oxygen and nickel peaks in the SIMS profiles obtained in grain boundaries (Fig. 6b) by the sputtering of a part of these nickel oxide particles.

*Complementary investigations.*—As the results obtained in this study are different from those achieved in the past, complementary investigations were made to look for further explanations. We have

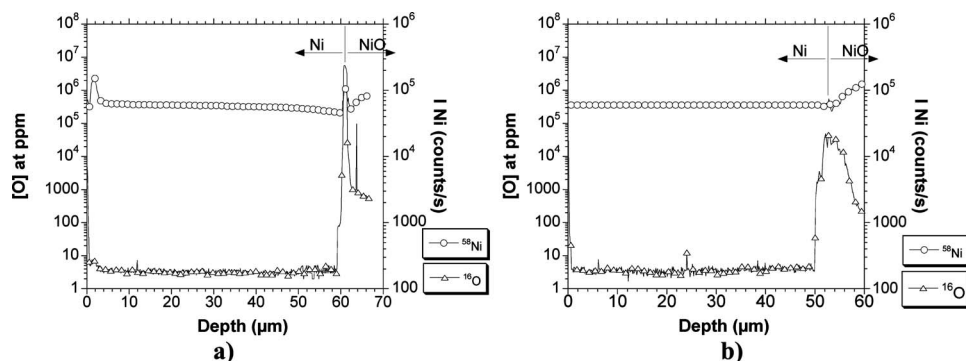


**Figure 9.** Reverse side SIMS profiles of  $^{16}\text{O}$  and  $^{58}\text{Ni}$  obtained in a 125- $\mu\text{m}$ -thick nickel foil-100 h/1000°C/Rhines Pack. (a) Profiles obtained in a metallic grain, (b) profiles obtained in a metallic grain boundary.

first focused on the cooling rate of the samples just after the oxidation treatment. Indeed, in the above experiments, SIMS analyses were made at room temperature on samples which had cooled down from 1000 to 25°C in a closed furnace. One can then imagine that during this air cooling, oxygen in a solid solution could have enough time to escape from the metallic bulk in agreement with the decrease of oxygen solubility in nickel with decreasing temperature.<sup>10</sup> 1-mm-thick samples were then water-quenched just after the oxidation treatment (48 h at 1000°C) and analyzed in the SIMS apparatus in the hour following the quenching. Again, oxide islands have been observed in the grain boundaries of the metal even if no oxygen diffusion has been measured in the concentration profile mode.

A second question must be asked concerning the results obtained above: as an oxide scale of several micrometers is formed on each sample at 1000°C, is not the consumption of metal at the metal-oxide scale interface (by the oxidation process) faster than the diffusion of oxygen in nickel? If yes, this could explain the very low content of oxygen in nickel measured by SIMS analysis. To answer this question, we have compared the thickness of the consumed metal as a function of time treatment with the hypothetical mean diffusion distance  $\sqrt{Dt}$  of oxygen in nickel, where  $D$  is the hypothetical diffusion coefficient of oxygen<sup>10</sup> ( $9.13 \times 10^{-9} \text{ cm}^2 \text{ s}^{-1}$ ) and  $t$  is the duration of the oxidation treatment. After 48 h at 1000°C, the mean diffusion distance is nearly equal to 400  $\mu\text{m}$ , which must be compared to the 35  $\mu\text{m}$  of nickel oxide formed during this treatment (i.e., to the 21  $\mu\text{m}$  metal surface recession). It then appears that the diffusion distance of oxygen in nickel calculated from the literature data should be much larger than the layer of metal consumed to form the external oxide scale.

125- $\mu\text{m}$ -thick samples of nickel have also been heat-treated at 1000°C in a sealed quartz tube (under secondary vacuum) in which a Rhines pack of a Ni/NiO powder mixture (0.5 g/0.5 g) had been first placed. The oxygen partial pressure is then fixed by the Ni/NiO mixture and is nearly equal to  $10^{-15} \text{ Pa}$  at 1000°C.<sup>35</sup> As a consequence, no continuous oxide layer is formed. The SIMS analyses of these heat-treated samples have led to the same results as those achieved for the oxidized specimen, proving that the oxygen species does not diffuse as expected in the grains of the metallic substrate (Fig. 9).

*Remark:* The relative humidity in the furnace was not checked. Errkik<sup>36</sup> has observed that the oxidation kinetics of nickel at 1000°C in dry and humidified air are quite comparable. The oxide has always been identified as fcc NiO and no differences in the microstructure of the oxide have been noticed. Wouters,<sup>37</sup> studying oxidation of nickel at 1000°C in dry air and in pure water vapor (133 mbar), has noticed a lower oxidation kinetics in pure water vapor but not in humidified air. In our study, the oxidation of nickel is realized in slightly humidified air (laboratory air). The oxide has been identified as fcc NiO by XRD, and measures of the oxide thickness after oxidation do not reveal lower oxidation kinetics than in dry air. Then we do not think that humidity could have an influence on our results except for the ratio  $p\text{O}_2/p\text{H}_2\text{O}$  many times lower than unity (which is not the case in the furnace). The oxygen partial

pressure at the Ni/NiO interface is fixed by the equilibrium between the metal and the oxide and can be determined using Ellingham diagrams (about  $10^{-15} \text{ Pa}$  at 1000°C).

### Discussion

Contrary to the internal oxidation method or coulometric titration, the SIMS technique with GDMS calibration allows a local and direct determination of the oxygen content in nickel in solid solution. As is clearly shown above, the oxygen content measured in metallic grains of high-purity polycrystalline foils (containing less than 100 atom ppm of metallic impurities) is the same before and after oxidation treatments in air at 1000°C. This is proof of the nondiffusion of oxygen in nickel grains or at least of the very low value of the diffusion coefficient at that temperature, or to the very low terminal solubility of oxygen in pure nickel. Indeed, taking into account the fact that in some cases oxygen diffusion can be suspected on distances lower than 1  $\mu\text{m}$  after 100 h at 1000°C, one can assert that the oxygen diffusion coefficient is lower than  $10^{-13} \text{ cm}^2 \text{ s}^{-1}$ , the alternative explanation being that oxygen does not diffuse because its maximum solubility in pure nickel at 1000°C is not more than 5 or 10 ppm. To explain the discrepancy between the results presented in this paper and previous ones (see the beginning of the paper), two principal aspects must be considered. The first one is the grain boundary diffusion. At this stage, and as it has been suggested in the Experimental section, we must indicate that the spatial resolution of the SIMS apparatus, in concentration profile mode or in imaging mode, is not sufficient (8  $\mu\text{m}$  in the first case and 0.1  $\mu\text{m}$  in the second one) to isolate a grain boundary whose width  $\delta$  is about 1 nm or less. Then the measured oxygen signal intensity comes from the grain boundary itself but also from the close environment of the grain boundary. The following modeling can be made. In imaging mode, a grain boundary of 1 nm width crossing one pixel of  $100 \times 100 \text{ nm}$  (Fig. 10a) accounts only for 1% of the analyzed surface area. Then, if the oxygen concentration in the 1 nm width region is the solubility limit determined by

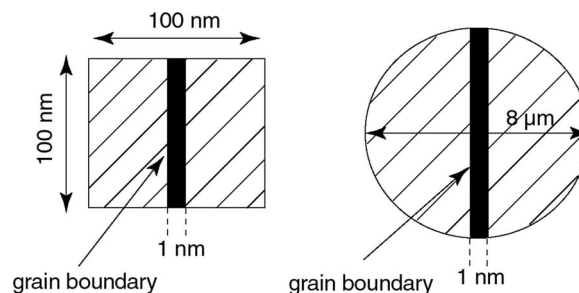


**Figure 10.** Sketches used for the modeling of the grain boundary diffusion of oxygen in nickel. (a) Grain boundary crossing a pixel in SIMS image mode, (b) grain boundary crossing the analyzed zone in SIMS concentration profile mode.

Park et al.,<sup>10</sup> i.e., 460 atom ppm, this would lead to an increase of the average concentration of the analyzed pixel zone from 5 to less than 10 atom ppm (or from 10 to 15 atom ppm). In image mode, a pixel containing a grain boundary would then be nearly two times brighter than its neighbor which does not contain any grain boundary. This brightness increase is clearly not sufficient to be detected in image mode.

The same quantification can be made for SIMS concentration profile mode (Fig. 10b). In this case, the analyzed region is an 8- $\mu\text{m}$ -diam disk (which is the diameter of the diaphragm used for the analysis). Then the measured oxygen concentration in a region containing a grain boundary saturated with 460 atom ppm of oxygen would be equal to 5.07 instead of 5 atom ppm (or 10.07 instead of 10 atom ppm). Again, the increase of the oxygen content (in comparison with a region which does not contain any grain boundary) is insufficient to be measured by the concentration profile mode.

This simple modeling shows that an exclusive diffusion of oxygen in nickel grain boundaries cannot be ruled out considering the lateral resolution of the SIMS technique. This is the only explanation to account for the results obtained by Park and Alstetter<sup>10</sup> by coulometric titration (see the beginning of the paper): in their study, one can imagine that the authors measure a very high oxygen flux in nickel grain boundaries under a voltage difference. This would be consistent with the hypothesis made by Bricknell and Woodford,<sup>3,4</sup> who explained the embrittlement of nickel following high-temperature exposure in air by the penetration of oxygen along grain boundaries. Oxygen is indeed suspected to be the species responsible for the pinning of the grain boundaries promoting ductility minima at high temperature (700–800°C).<sup>3,4</sup>

Second, concerning the internal oxidation method used to determine the oxygen diffusion in nickel,<sup>11–17</sup> the presence of additions such as chromium, beryllium, or silicon may have a great influence on oxygen diffusivity in nickel as the results are quite different from those obtained in high-purity samples using the SIMS technique for the analysis. However, in the present study, the occurrence of NiO particles in metallic grain boundaries (several hundred micrometers under the metal/oxide scale interface) after oxidation treatments must be cleared up. In a previous paper,<sup>38</sup> it has been shown that many voids nucleate in metallic grain boundaries when the two faces of nickel samples are oxidized. Furthermore, the demonstration has been made that some of the metallic vacancies formed at the metal/oxide scale interface were deeply injected in the metallic grain boundaries and annihilated in these voids, leading to the growth of these defects. A void, located 200  $\mu\text{m}$  under the metal/oxide scale interface, has been marked out by a Vickers indentation before the SIMS analysis of the sample in image mode. The images obtained show that the void corresponds to a NiO particle, proving the fact that the walls of the voids are oxidized. This has been confirmed by TEM analysis, using EDX and electronic diffraction. The formation of nickel oxide particles in the bulk of a pure nickel sample is in contradiction with the classical Wagner's theory of internal oxidation.<sup>21</sup> But, one can imagine a transport of the oxygen species by nickel vacancies leading to a nonequilibrium increase of the oxygen partial pressure in the voids (where the vacancies are annihilated) and then to this internal oxidation due to oxygen oversaturation in the grain boundaries. Calculations at the atomic scale are in progress to verify if the oxygen diffusion in nickel can be accelerated by the presence of metallic vacancies which could lower the activation energy in the expression of the diffusion coefficient.

### Conclusion

SIMS analysis made on samples of high-purity polycrystalline nickel foils oxidized at 1000°C in laboratory air have shown that the oxygen solubility in grains of nickel was much lower than values obtained in previous works (50 to 100 times lower at least). Furthermore, the diffusion of the oxygen species in the metallic grains is not evidenced over distances higher than 1  $\mu\text{m}$  even

after oxidation treatment duration of 100 h: this result is in contradiction with diffusion calculations derived from the literature data. However, taking into account the lateral resolution of the SIMS technique (higher than 0.1  $\mu\text{m}$ ), an exclusive diffusion of oxygen in nickel grain boundaries cannot be ruled out: this could partly explain the discrepancy between the results obtained in this study and previous ones. The oxygen diffusion would then exclusively occur in the grain boundaries. This remark is reinforced by the fact that a few NiO particles have been exclusively observed at grain boundaries after the oxidation treatment. This last observation is in contradiction with the classical internal oxidation theory and can only be explained by an oversaturation of oxygen at grain boundaries. The intergranular oxygen diffusion could be accompanied by a local enrichment, which is really difficult to measure directly. As has been already demonstrated indirectly,<sup>3</sup> this local segregation can generate an interfacial embrittlement partly responsible for the loss of ductility reported for nickel-based alloys at high temperature. Moreover, as is suggested in this paper, the oxygen flux in the metal is strongly dependent on the existence of vacancy sinks in the grain boundaries such as voids or internal oxides of less noble metals.

Investigations are in progress to go further in the understanding of the mechanisms and to propose an enriched database of the oxygen diffusion in nickel.

### Acknowledgments

The authors express their gratitude to M. C Lafont, C. Armand, and J. P Bonino for the TEM, SIMS, and interferometry analysis.

CIRIMAT/ENSIACET assisted in meeting the publication costs of this article.

### References

1. C. G. Bieber and R. F. Decker, *Trans. Metall. Soc. AIME*, **221**, 629 (1961).
2. F. N. Rhines and P. J. Wray, *Trans. Am. Soc. Met.*, **54**, 117 (1961).
3. R. H. Bricknell and D. A. Woodford, *Metall. Trans. A*, **12**, 425 (1981).
4. R. H. Bricknell and D. A. Woodford, *Met. Sci.*, **18**, 265 (1984).
5. E. P. Simonen, L. E. Thomas, and S. M. Brummer, *Corrosion Cracking International Conference*, p. 226, American Society for Metals, Materials Park, OH (2000).
6. R. W. Staehle and Z. Fang, *Ninth International Symposium on Environmental Degradation of Materials in Nuclear Power Systems*, p. 69, The Minerals, Metals, and Materials Society, Warrendale, PA (1999).
7. P. M. Scott and M. L. Calvar, *6th Proceedings of the International Symposium on Environmental Degradation of Materials in Nuclear Power Systems—Water Reactors*, p. 657, The Minerals, Metals, and Materials Society, Warrendale, PA (1993).
8. A. U. Seybolt and R. L. Fullman, *Trans. Am. Inst. Min., Metall. Pet. Eng.*, **200**, 548 (1954).
9. C. B. Alcock and P. B. Brown, *Met. Sci. J.*, **3**, 116 (1969).
10. J. W. Park and C. J. Alstetter, *Metall. Trans. A*, **18A**, 43 (1987).
11. R. Barlow and P. J. Grundy, *J. Mater. Sci.*, **4**, 797 (1969).
12. S. Goto, K. Nomaki, and S. Koda, *J. Jpn. Inst. Met.*, **31**, 600 (1967).
13. G. J. Lloyd and J. W. Martin, *Met. Sci. J.*, **6**, 7 (1972).
14. G. J. Lloyd and J. W. Martin, *Met. Sci. J.*, **7**, 75 (1973).
15. J. L. Meijering and M. J. Druyvesteyn, *Philips Res. Rep.*, **2**, 81 (1947).
16. C. J. Smithells and C. E. Ransley, *Proc. R. Soc. London, Ser. A*, **155**, 195 (1936).
17. G. Grigorev and L. Pavlinov, *Fiz. Met. Metalloved.*, **25**, 836 (1968).
18. P. Kofstad, *High Temperature Corrosion*, p. 251, Elsevier Applied Science, London (1988).
19. M. J. Graham and R. J. Hussey, *Corros. Sci.*, **44**, 319 (2002).
20. J. Mao and R. B. McLellan, *J. Phys. Chem. Solids*, **64**, 527 (2003).
21. C. Wagner, *Z. Elektrochem.*, **63**, 772 (1959).
22. R. A. Rapp, *Acta Metall.*, **9**, 730 (1961).
23. D. Bruce and P. Hancock, *J. Inst. Met.*, **97**, 148 (1969).
24. N. Birks and G. H. Meier, *Introduction to High Temperature Oxidation of Metals*, p. 69, Edward Arnold Ltd., London (1983).
25. S. Perusin, B. Viguier, J.C. Salabura, D. Oquab, and E. Andrieu, *Mater. Sci. Eng., A*, **387–389**, 763 (2004).
26. R. Peraldi, D. Monceau, and B. Pieraggi, *Oxid. Met.*, **58**, 249 (2002).
27. R. Peraldi, D. Monceau, and B. Pieraggi, *Oxid. Met.*, **58**, 275 (2002).
28. S. Perusin, B. Viguier, D. Monceau, and E. Andrieu, *Mater. Sci. Forum*, **461–464**, 123 (2004).
29. M. Aucouturier, G. Blaise, and E. Darque-Ceretti, *Microcaractérisation des Solides—Méthodes d'Observation et d'Analyse*, p. 336, Michel Amou, Editor, CRAM CNRS, Paris (1989).
30. G. Moulin, P. Arevalo, and A. Salleo, *Oxid. Met.*, **45**, 153 (1996).
31. F. N. Rhines, R. G. Connell, and M. Choi, *J. Electrochem. Soc.*, **126**, 1061 (1979).
32. J. Panter, Ph.D. Thesis, Institut National Polytechnique de Toulouse, Toulouse (2002).

33. J. Panter, B. Viguier, J. M. Cloué, M. Foucault, P. Combrade, and E. Andrieu, *J. Nucl. Mater.*, to be submitted.
34. J. P. Eberhart, *Analyse Structurale et Chimique des Matériaux*, p. 431, Dunod, Paris (1997).
35. I. Barin, *Thermochemical Data of Pure Substances*, Vol. 2, p. 1067, VCH, Weinheim (1993).
36. A. Errkik, Ph.D. Thesis, UTC Compiègne, p. 126 (1995).
37. Y. Wouters, Ph.D. Thesis, p. 189, Institut National Polytechnique de Grenoble, Grenoble, France (1992).
38. S. Perusin, B. Viguier, D. Monceau, L. Ressler, and E. Andrieu, *Acta Mater.*, **52**, 5375 (2004).